Open Journal of Marine Science, 2026, 16(4), 178-191
https://www.scirp.org/journal/ojms
ISSN Online: 2161-7392
ISSN Print: 2161-7384

Resilience or a Trend towards the Weakening of the Cold Water Tongue under the Influence of Local Warming?

Mamadou Koné[1]*, Yves Kouadio[2], Hubertine Doulou[2]

[1]Training and Research Unit of Marine Sciences, University of San-Pédro, San-Pédro, Côte d'Ivoire
[2]Laboratory of Matter Sciences, Environment and Solar Energy (LASMES), University F.H.B. of Cocody-Abidjan, Abidjan, Côte d'Ivoire
Email: *konemamadou884@gmail.com

How to cite this paper: Koné, M., Kouadio, Y. and Doulou, H. (2026) Resilience or a Trend towards the Weakening of the Cold Water Tongue under the Influence of Local Warming? *Open Journal of Marine Science*, **16**, 178-191.
https://doi.org/10.4236/ojms.2026.164011

Received: June 6, 2026
Accepted: August 8, 2026
Published: August 11, 2026

Abstract

The equatorial Atlantic cold water tongue plays a key role in regulating the climate of the West African continent and the marine ecosystems of the equatorial Atlantic. This study examines its vulnerability to the increasing frequency of marine heatwaves between 1993 and 2025. Using an approach combining climatological analyses and decomposition into empirical orthogonal functions, we quantify the spatiotemporal evolution of its cooling surface. The results reveal a marked spatial asymmetry, with the central and western equatorial sector (15˚W - 5˚W) emerging as the dynamic core of the system, but also proving to be the most vulnerable to thermal contractions. Event-based analysis shows that the presence of significant negative anomalies (−68.000 km^2) two weeks prior to the peak of marine heatwaves highlights a preconditioning effect, whereby a prior weakening of upwelling facilitates the triggering of the heatwave. During marine heatwaves, the average reduction reaches −110.000 km^2. The key finding lies in the post 2015 break, manifested by the ongoing transition of the primary mode of variability (71.5 per cent of the variance) towards a state of chronic contraction. Coupled with incomplete resilience during the relaxation phase (−56.000 km^2), this trend shows that, under the influence of local warming and increased stratification, the thermocline's readjustment time now exceeds the return period of the MHWs. Rather than merely a temporary resistance, the cold water tongue is undergoing a chronic spatial decline, ultimately threatening the regional biogeochemical balance.

Keywords

Cold Water Tongue, Marine Heatwaves, Upwelling, Stratification, Climate

Change

1. Introduction

Over recent decades, anthropogenic climate change has led to unprecedented warming of the upper layers of the global ocean, profoundly altering heat fluxes and fluid dynamics on a global scale [1] [2]. This global thermal forcing is now compounded by an increase in extreme weather events. Among these are Marine Heatwaves (MHWs). MHWs are standardised as prolonged positive anomalies in sea surface temperature (SST) exceeding the 90th historical percentile for at least five consecutive days [3]. In recent years, they have emerged as a crucial area of study in oceanography. These events, once considered exceptional, are seeing their frequency, peak intensity and duration increase continuously across the globe as a result of thermodynamic feedback from the atmosphere [4].

Against this backdrop of widespread thermal anomalies, the tropical Atlantic Ocean and more specifically the Gulf of Guinea (GoG) is experiencing an alarming increase in the frequency of these thermal extremes [5]-[7]. The occurrence of these repeated MHWs is likely to severely disrupt regional hydrodynamic systems, particularly upwelling processes [5]. Whilst the GoG is home to several cold-water upwelling systems, including coastal upwellings (the Ivorian Ghanaian, Congo Gabonese and Benguela upwellings), this study focuses on equatorial upwelling, a major dynamic structure known as the Atlantic Cold Tongue (ACT) during MHWs. The ACT is a major seasonal thermal structure that extends along the equator (generally between 20˚W and 0˚E) and peaks during the northern hemisphere summer, from June to September [8]. This is a region whose dynamics are governed by a highly non-linear ocean atmosphere coupling, analogous to the Bjerknes mechanism described in the Pacific [9] [10]. Under the influence of the south-easterly trade winds, which strengthen during the northern hemisphere spring, equatorial Ekman divergence and wind stress force the upwelling of cold, nutrient-rich subsurface waters [11] [12]. This upwelling process is intrinsically linked to the vertical structure of the open ocean, in particular to fluctuations in the thermocline slope induced by the propagation of equatorial planetary waves Kelvin and Rossby waves [13] [14] and to the horizontal advection associated with the Equatorial Undercurrent (EUC), a powerful eastward-flowing subsurface jet [15]-[17]. However, this seasonal cycle plays a fundamental role in regulating temperature and climate on a continental scale [8]. The thermal gradient that develops between the ACT and the overheated West African continent constitutes the essential thermodynamic driver for the onset and penetration of the West African monsoon, thereby modulating precipitation patterns across West Africa [8] [18] [19]. At the same time, the influx of nutrients into the euphotic zone makes this region one of high primary productivity, supporting the upper food webs and the vital fisheries of the countries bordering the GoG [20]. However, intensifying local warming, combined with the occurrence of MHWs which are often modulated by interannual variability linked to the Atlantic Zonal Mode or Atlantic El Niño [21] [22] now threatens to disrupt the delicate physical balance that governs this structure. Whilst the characteristics of MHWs are increasingly well documented by satellite observations in this region, their impact on the intrinsic dynamics of the EAT remains largely unknown. Most existing studies are limited to a descriptive statistical characterisation of surface MHWs, neglecting to analyse their impacts on the seasonal cooling of the Equatorial Atlantic. It is precisely this scientific gap that this research addresses. The main objective of this study is to assess the impact of MHWs on the spatial extent of the ACT over the last three decades. To this end, we employ robust statistical methods, including the standardised detection algorithm developed by Hobday *et al.* [3] and empirical orthogonal functions. Ultimately, the aim is to determine whether the ACT retains its capacity for dynamic resilience, or whether it is heading towards chronic and structural weakening under the influence of increasingly intense and invasive MHWs.

2. Data and Methods

2.1. Study Area

The Equatorial Atlantic is a fascinating region of the Atlantic Ocean that extends on either side of the equator between 5˚N and 5˚S (**Figure 1**). It is a crucial transition zone connecting the North Atlantic and the South Atlantic, playing a key role in regulating the West African climate [8]. From an oceanographic perspective, this zone is particularly dynamic and complex, with a current system comprising major currents such as the northern and central branches of the South Equatorial Current (nSEC and cSEC), which drive surface waters westwards [16]. Just below this flows the Equatorial Undercurrent (EUC), a veritable underwater river moving in the opposite direction, towards the east. Furthermore, due to the Coriolis force which cancels itself out at the equator but deflects the waters just to the north and south the surface waters diverge. This causes deep, cold and nutrient-rich waters to upwelling, a phenomenon particularly evident in the GoG during the summer [8].

2.2. Data

The temperature data used in this study are taken from the Copernicus Marine Environment Monitoring Service's global ocean reanalysis (product GLOBAL_MULTIYEAR_PHY_001_030, dataset cmems_mod_glo_phy_my_0.083deg_P1D-m) at 5 m. These daily mean fields, based on the MERCATOR GLORYS12V1 configuration from Mercator Ocean, provide a global simulation at a high spatial resolution of 1/12˚ (approximately 8 km). These data were extracted via the Marine Data Store's MyOcean portal from the Copernicus Marine at https://data.marine.copernicus.eu/viewer/expert/. They have been the subject of several studies in the Atlantic, such as those by Qingyang Song and Hidenori Aiki [23], and are sufficiently well characterised in this oceanic region by the work of Drévillon *et al.* [24].

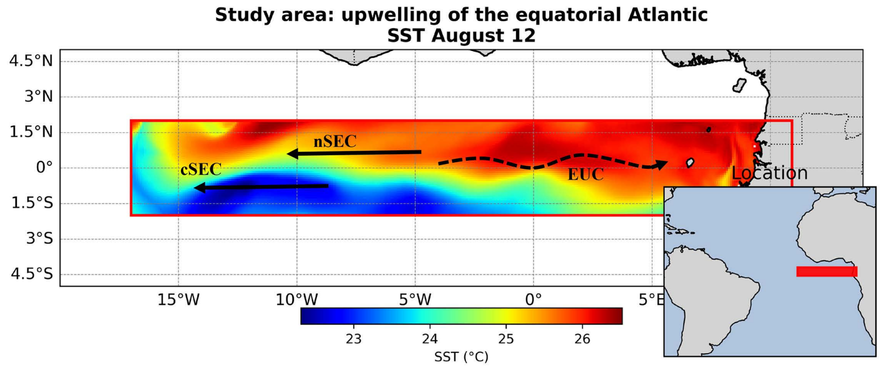

Figure 1. Map of the Atlantic with a close-up of the tropical Atlantic. The area outlined in red represents the study area, showing the average daily temperature on 12 August 2012, with the northern and central branches of the South Equatorial Current shown as solid lines flowing westwards and the Equatorial Counter-Current shown as a dotted line flowing eastwards. South Equatorial Current (nSEC and cSEC) and Undercurrent (EUC).

2.3. Methods

2.3.1. Calculation of the Cooling Surface

To determine the cooling surface area, the methodology developed by Caniaux *et al.* [8] was applied. This approach involves integrating, on a daily basis, the area of all grid cells where the SST is below a predefined threshold value, using the formula below. This thermal threshold is set at 25˚C, a characteristic value as it is lower than the average ocean temperature measured in June in the eastern equatorial Atlantic, a key period for the development of upwelling [8]. According to these same authors, the cumulative area thus obtained must exceed a critical threshold set at 0.40106 km^2.

$$US = \int_{A(x)} H_e\left(25^{\circ}\mathrm{C} - \mathrm{SST}(x)\right) dA \quad [8]$$

where US is the upwelling area, H_e is the Heaviside function ($H_e = 1$ when SST < 25˚C and 0 otherwise), A is the domain from 17˚W to 12˚E and from 2˚S to 2˚N, and SST is the daily mean temperature.

Secondly, the daily surface anomaly is simply the difference between the observed surface value and the climatological value for the corresponding calendar day. This climatology is established over the entire study period (1993-2025). Thus, a positive anomaly indicates an upwelling area greater than the daily normal, whilst a negative anomaly indicates a deficit relative to this reference.

2.3.2. Empirical Orthogonal Functions

To analyse the spatio-temporal variation in the upwelling area, we used Empirical Orthogonal Function (EOF) analysis. This method, which is an extension of Principal Component Analysis (PCA) to spatio-temporal fields, has established itself as a robust statistical tool in oceanography and climatology. It enables the dimensionality of large, multidimensional datasets to be reduced by decomposing the signal into orthogonal modes of variability [25]. These modes, ranked according to their contribution to the total variance of the system, allow spatial structures and their associated temporal amplitude coefficients to be isolated [26]. In practice, most of the physical variance is concentrated in the first three or four modes, which capture the dominant dynamic processes, whilst higher-order modes are generally regarded as background noise. Readers may find further details on this method in the work of Shields *et al.* [26].

2.3.3. Detection of MHW Periods

To analyse the impact of MHWs on the upwelling area, we determined the MHW period using the method developed by Hobday *et al.* [3], which has become the international standard in oceanography [4]. It is based on a rigorous statistical approach that enables events to be identified from daily temperature time series spanning at least 30 years [27]. This approach, which has already been validated in the tropical Atlantic for the study of MHWs, is based on the definition of a moving seasonal climatology and a temperature threshold set at the 90th percentile of the local historical distribution [5]-[7]. For the present study, the impact of MHWs on the upwelling area is examined over the fifteen days preceding, during and the fifteen days following the MHW period. The choice of this time window is based on the work of Garfinkel *et al.* [28], which demonstrates that such a duration allows for the optimal capture of the responses of oceanic parameters induced by MHWs. This approach is also consistent with the methodologies used in recent studies of the region, which analyse oceanic and atmospheric conditions before, during and after MHW events in order to understand their impacts [5] [6]. In order to confirm the statistical robustness of the impact of MHWs on the ACT, a composite approach is applied over the period 1993-2025, supported by a non-parametric bootstrap analysis (2.000 resamples) of the detected MHW events, providing 95 per cent confidence intervals for each phase.

3. Results

3.1. Spatio-Temporal Variability in the Area of Cold Water Tongue from 1993 to 2025

The Hovmöller plots (**Figure 2**) show the seasonal and interannual variability in the spatio-temporal extent of the cooling (expressed as area: 10^6 km^2) within the cold water tongue region (17˚W - 12˚E and 2˚S - 2˚N) from 1993 to 2025.

Figure 2(a) shows an extremely pronounced and regular seasonal pattern of the cold-water tongue throughout the 33 years of observation. It indicates that the cooling begins to manifest itself tentatively in May (M), intensifies rapidly in June (J) to reach its maximum spatial extent in July (J) and August (A), with cooling areas regularly exceeding 70.10^6 km^2 to 80.10^6 km^2. A relaxation phase is also observed in September (S), followed by an almost complete disappearance of the surface signature between October (O) and April (A). This behaviour is consistent with the classic dynamics of upwelling induced by the seasonal strengthening of the trade winds. **Figure 2(a)** reveals significant interannual variability, resulting in years of intense upwelling during the period 1993-2006. Conversely, several years, such as 2007, 2008, 2016 and 2021, show a dramatic weakening of the cooling surface area, with values rarely exceeding 50 - 60 × 10^6 km^2, indicating weak or aborted upwelling. Figure 2(b), which shows the evolution of the area as a function of longitude and time, highlights a marked east-west asymmetry in the extent and intensity of the cooling. Figure 2(b) reveals that the centre of the cooling is located between 15˚W and 5˚W. Indeed, in this zone the cooling is at its maximum, covering an area of 7.000 to over 10.000 km^2. Moving eastwards towards 3˚W to 10˚E, the extent of the cooling decreases drastically (<4.000 km^2). The interannual variability shown in this figure indicates that the period 1993-2005 was one in which the western core was particularly active. During this period, two major peaks in extent were observed: in 1993-1997 and, in particular, between 2000 and 2002, when the area exceeded 10.000 km^2. Furthermore, a second period, 2006-2015, corresponds to a transitional phase during which the core remained stable around 10˚W, with a notable secondary peak in 2013-2014. However, the overall spatial extent is slowly beginning to contract horizontally compared with the previous decade. A break is observed in 2016, with the core at 10˚W almost completely disappearing between 2016 and 2023 halving the cooling area, which falls below 6.000 km^2. From 2024 to 2025, a rebound is observed, corresponding to a sudden resurgence of cooling towards the end of the 2025 period, centred on 10˚W.

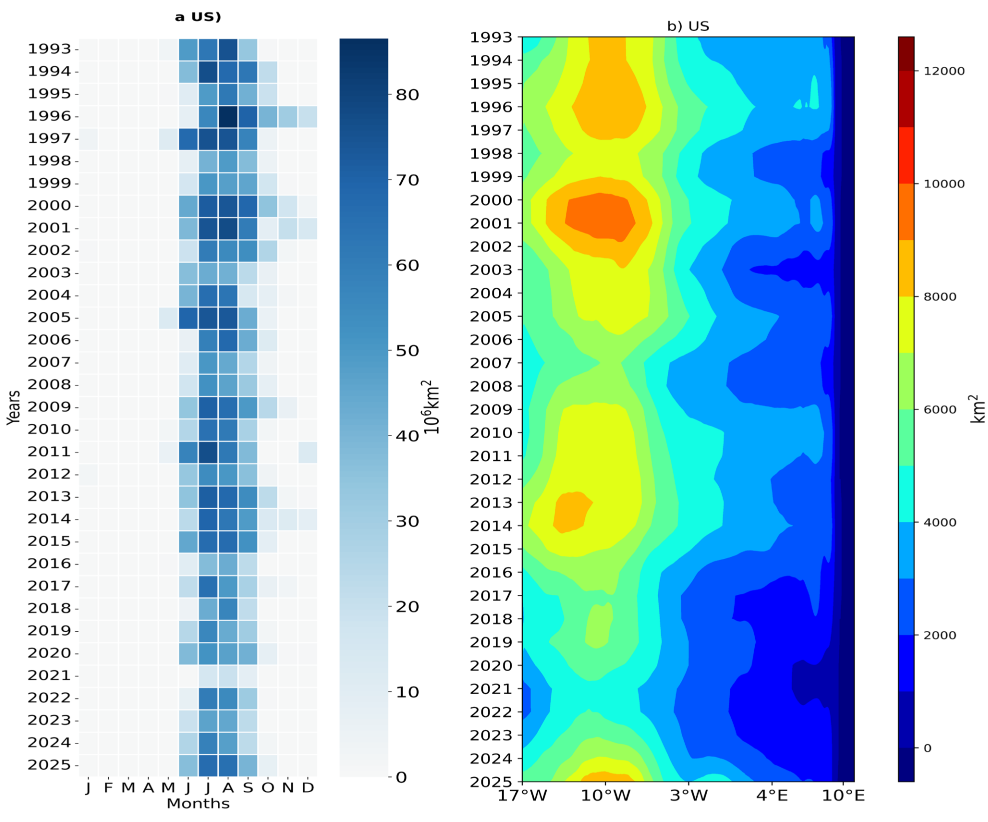

Figure 2. Hovmöller plot of the upwelling surface (US) of the ACT by month-year (a) and longitude-year (b) during the period 1993-2025.

3.2. Principal Modes of Variability of Cold Water Tongue from 1993 to 2025

Applying EOF analysis to our time series from 1993 to 2025 enabled us to extract the principal modes of variability of the ACT surface over this period. Of the modes obtained, only the first three were retained, as they account for the majority of the system's total variance. The first mode (**Figure 3(a)**, EOF1, 71.5% of variance) reveals an overall negative signal across the entire basin, with values ranging from 0 to −2.450 km^2 and maximum amplitude at the heart of the cold water tongue. This mode represents an overall contraction or suppression of upwelling. PC1 (**Figure 3(d)**) shows a dramatic interannual transition: prior to 2015, it indicates a signal with strongly negative values (1996, 2000), which, when combined with the negative spatial pattern, points to phases of very widespread upwelling. From 2016 onwards, PC1 becomes almost consistently positive, peaking at an absolute maximum in 2021. A positive PC1 multiplied by a negative EOF1 yields a strongly negative result, indicating a drastic and continuous reduction in the area of upwelling over the past decade. Furthermore, Mode 2 (**Figure 3(b)**, 9.4% of the variance) reveals, through its spatial structure (EOF2), a very distinct zonal dipole. This dipole is characterised by negative anomalies in the west (−800 km^2) and positive anomalies in the east, near the African coast (+1.200 km^2). The PC2 (**Figure 3(e)**) of this mode captures high-frequency variability with marked oscillations in 1993, 1996, 2005, 2010 and 2021, with strong positive peaks, and in 1998, 2000 and 2002, with negative peaks. Furthermore, mode 3 (**Figure 3(c)**, 4.3 per cent of the variance) has a spatial structure (EOF3) that shows a meridional banding pattern or a heart-shaped pattern. The centre of the ACT exhibits positive values of over 1.200 km^2, whilst the northern and southern edges (particularly in the south-west) show negative values exceeding −300 km^2. The PC3 (**Figure 3(f)**) associated with this mode shows high variability with extreme phases, particularly at the very start of the 1993 period, and marked troughs in 1999 and 2014.

3.3. Trends in the Cold Water Tongue before, during and after the MHWs from 1993 to 2025

To characterise the direct impact and temporal signature of MHWs on the ACT, surface upwelling anomalies were composite analysed according to three key phases (**Figure 4**). However, MHW events separated by ≤2 days were merged into a single episode; the others, including those with overlapping Before/After windows, were retained individually for the composites.

The first phase is the precursor phase, corresponding to 15 days before the MHWs, and it shows that the negative anomaly is often already present 15 days before the MHW, with the exception of the years 1994, 1996, 2009, 2010, 2013, 2014, 2022 and 2025. This indicates that the ACT was already weakening, creating conditions conducive to the onset of the MHWs. During the MHWs, the surface deficit of the cold-water tongue reaches massive proportions. Historical lows were recorded in 2007, with a record collapse of over −30.000 km^2, in 1999 at around

−230.000 km², in 2003 at over −250.000 km² and, more recently, in 2021 at around −270.000 km². Values recorded after MHWs are almost always higher than those recorded during MHWs. This shows a tendency towards resilience: once the MHWs have ended, upwelling tends to resume and reduce its negative anomaly. However, recovery is rarely complete; values remain negative, often fluctuating between −50.000 and −100.000 km², indicating a thermal memory effect in the surface ocean, which takes time to dissipate the accumulated heat. Furthermore, prior to 2015, the significant events were distinct but spaced out over time (1999, 2003 and 2007).

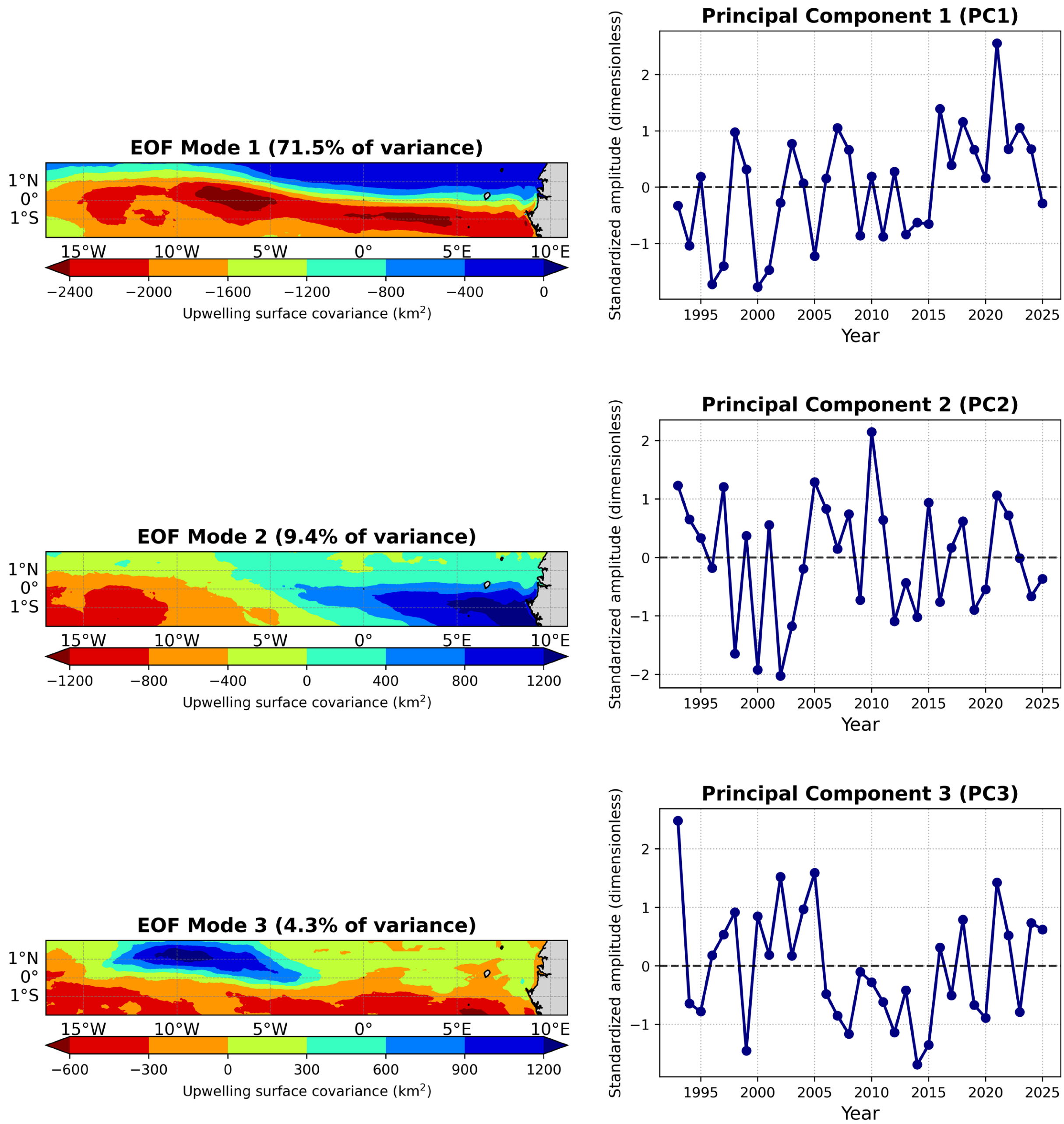

Figure 3. Spatio-temporal trends in the main modes of variability of the Equatorial Atlantic CTD surface from 1993 to 2025.

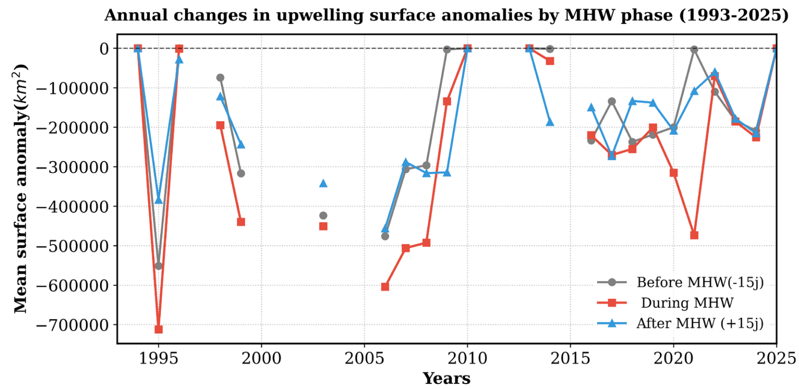

Figure 4. Changes in the ACT area 15 days before the MHWs (grey curve plus circle), during the MHWs (red curve plus square) and 15 days after the MHWs (blue curve plus triangle) from 1993 to 2025. The horizontal dotted line indicates the zero value.

3.4. Composite of the Cold Water Tongue before, during and after the MHWs from 1993 to 2025 Based on Bootstrap Resampling

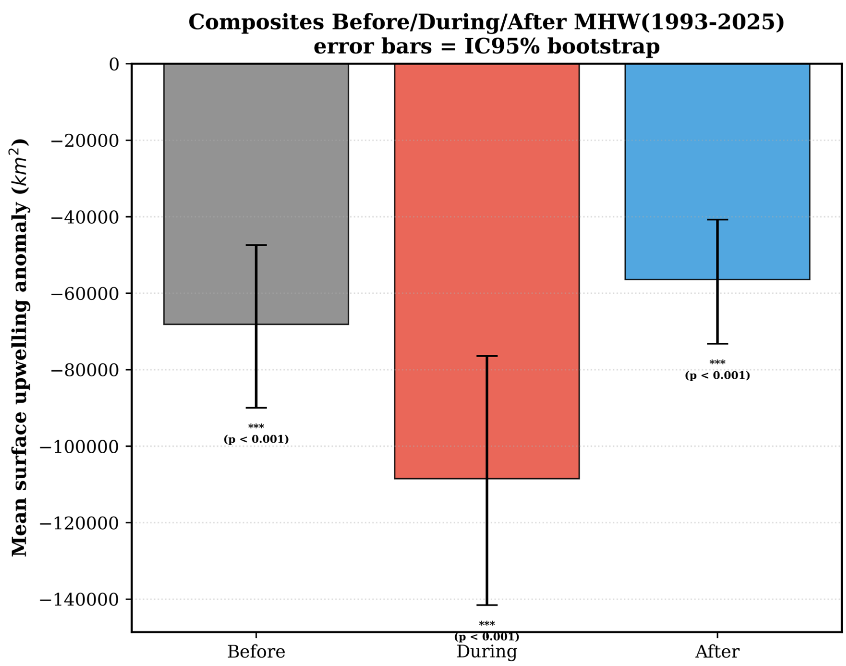

Figure 5. Composite of the ACT surface based on bootstrap resampling 15 days before the MHWs (grey box), during the MHWs (red box) and 15 days after the MHWs (blue box) during the period 1993-2025. The vertical lines represent error bars and the (p) values correspond to p-values.

In order to confirm the statistical robustness of the impact of MHWs on the ACT, a composite windowing tool combined with a bootstrap resampling method (95% CI, n = 2.000) was applied across the entire 1993-2025 period. The results (**Figure 5**) demonstrate with high statistical significance ($p < 0.001$) that MHWs are accompanied by a systematic collapse in the upwelling area. During the pre-event phase (Before), the average negative anomaly is already nearly −68.000 km^2. During the active phase (During), which corresponds to the peak of the impact, MHWs reduce the ACT by an average of nearly −110.000 km^2 over the entire study period. Finally, the post-event phase (After) shows a persistent anomaly of −56.000 km^2. Although there is a marked improvement compared with the active phase, the anomaly does not return to zero. Furthermore, for all three phases, the anomaly is significantly different from zero with a confidence level of over 99.9 per cent ($p < 0.001$). The error bars for the "Before" phase (from −47.000 to −90.000 km^2) and the "After" phase (from −40.000 to −73.000 km^2) overlap considerably; by contrast, the amplitude of the "During" phase extends much further down to −142.000 km^2.

4. Discussion

This study, which examines the resilience or weakening of the ACT under the influence of the warming observed in recent years, began with an analysis of the temporal distribution of the ACT extent (**Figure 1**). This analysis highlights the robustness of the seasonal cycle of the cold water tongue, the extent of which invariably peaks in July and August due to the strengthening of the trade winds and the onset of the monsoon [21]. However, this basic climatological signal is subject to significant interannual variability, with years of intense upwelling, such as 1996 or 2000, alternating with "warm spells" characterised by a drastic reduction in surface cooling, such as in 2016 or 2021. When the longitudinal dimension is taken into account (**Figure 2**), it can be seen that this weakening is not uniform, but reveals a clear east-west spatial asymmetry. The central and western equatorial sector (15˚W - 5˚W) stands out as the true thermal and dynamic heart of the ACT. It is precisely in this transition zone, where the thermocline normally begins to deepen towards the west that the system is at its most vulnerable, undergoing the most severe spatial contractions during warm anomalies. Furthermore, to better isolate the driving mechanisms behind this variability, the EOF decomposition (**Figure 3**) formalises these dynamics through three principal modes. The first mode (EOF1, 71.5% variance) reflects an overall, homogeneous negative thermal constraint, the principal component of which (PC1) reveals an abrupt break observed after 2015. The onset of a quasi-permanent positive phase of PC1 after 2015 is consistent with the results of Koné *et al.* [5]. This result demonstrates that the ACT is shifting towards a new, altered mean state, driven by global warming and increased vertical stratification of the mixing layer [1] [29]. This background signal is modulated at high frequency by the second mode (EOF2, 9.4% variance), which captures a dynamic zonal oscillation (east-west dipole). This oscillation mode, governed by wave-wind interactions and Bjerknes feedbacks [9] [30], dictates the fine-scale geographical structure of upwelling and shifts the thermal front of the ACT in response to equatorial Kelvin wave forcing. Mode 3, although minor in terms of explained variance (4.3%), reveals a mechanism for morphological adjustment of the ACT. The dipolar spatial structure of EOF3 suggests a process of contraction or pulsation of the ACT, rather than simply uniform warming. Positive phases of EOF3 correspond to a concentration of the ACT in its central region, whilst negative phases result in an expansion towards the periphery, particularly to the south-west. PC3 shows a strong interannual signal, with major negative anomalies coinciding with years of intense upwelling or abnormal wind forcing. To better understand the evolution of the ACT, an event-scale analysis (**Figure 4**) enabled the spatial structures of the ACT to be directly linked to the chronology of MHWs on a year-by-year basis, covering the weeks before, during and two weeks after. The superimposition of these phases highlights the ocean's role as a preconditioner over the selected time interval. Indeed, the systematic presence of negative surface anomalies 15 days before the peak of the MHWs (the "Before" phase) suggests that a prior weakening of upwelling dynamics whether through wind relaxation or warm-structure waves sets the stage for the triggering of the MHWs [31]. However, whilst the active phase of the event (During) causes an immediate and maximal collapse of the ACT, sometimes exceeding –250.000 km^2, the relaxation phase (After) shows incomplete recovery, confirming that a warm thermal signature persists in the mixing layer well after the end of the crisis [32]. Finally, the synthesis of these processes is statistically validated by the global composite analysis (**Figure 5**). By quantifying the average area losses over the three decades, the bootstrap analysis confirms with a high level of significance ($p < 0.001$) the destructive impact of the MHWs, which reduce the ACT by an average of nearly −110.000 km^2 at their peak. Furthermore, the persistence of an average deficit of −56.000 km^2 in the post-event phase provides statistical evidence of a memory effect or thermal hysteresis. Furthermore, a post 2015 climate regime has been identified, characterised by a sharp increase in the frequency of MHWs [4], with the thermocline taking more than two weeks to readjust, which could lead to a chronic and permanent contraction of the ACT.

5. Conclusion

Ultimately, these results suggest that the ACT is no longer merely experiencing transient warm anomalies, but is evolving towards a chronic and structural reduction in its surface area. In the future, this change in the mean state of the surface ocean could profoundly alter ocean-atmosphere coupling at the regional scale, disrupt the African monsoon and have severe ecological and socio-economic consequences for marine ecosystems and local fisheries.

Author Contributions

Conceptualization, M.K.; Y.K.; methodology, M.K., Y.K., D.H.; formal analysis M.K.; writing—original draft preparation, M.K., D.H., Y.K.; writing-review and editing, M.K, D.H., Y.K., supervision, Y.K. All authors have read and agreed to the published version of the manuscript.

Conflicts of Interest

The authors declare no conflicts of interest regarding the publication of this paper.

References

[1] Oliver, E.C.J., Donat, M.G., Burrows, M.T., Moore, P.J., Smale, D.A., Alexander, L.V., *et al.* (2018) Longer and More Frequent Marine Heatwaves over the Past Century. *Nature Communications*, **9**, Article No. 1324. https://doi.org/10.1038/s41467-018-03732-9

[2] Legg, S. (2021) IPCC, 2021: Climate Change 2021: The Physical Science Basis. *Interaction* (*Melbourne*), **49**, 44-45. https://research.ebsco.com/c/4rzq2t/search/details/aeuakdp5qr?ampSessionId=1785918591403&ampDeviceId=f52ed69e-0ba3-4372-8d06-9066282f1ac8&request-context=plink&db=aph

[3] Hobday, A.J., Alexander, L.V., Perkins, S.E., Smale, D.A., Straub, S.C., Oliver, E.C.J., *et al.* (2016) A Hierarchical Approach to Defining Marine Heatwaves. *Progress in Oceanography*, **141**, 227-238. https://doi.org/10.1016/j.pocean.2015.12.014

[4] Oliver, E.C.J. (2019) Mean Warming Not Variability Drives Marine Heatwave Trends. *Climate Dynamics*, **53**, 1653-1659. https://doi.org/10.1007/s00382-019-04707-2

[5] Koné, M., Djakouré, S., Adon, M., Ta, S. and Kouadio, Y. (2022) Marine Heatwaves, Upwelling, and Atmospheric Conditions during the Monsoon Period at the Northern Coast of the Gulf of Guinea. *Climate*, **10**, Article 199. https://doi.org/10.3390/cli10120199

[6] Djakouré, S., Koné, M., Koffi, K.U., Kouadio, K.Y., Adon, M., Nyadjro, E., *et al.* (2023) Characterization of Marine Heat Waves in the Eastern Tropical Atlantic Ocean. *Frontiers in Marine Science*, **10**, Article 1293779. https://doi.org/10.3389/fmars.2023.1293779

[7] Koné, M., Kouadio, Y.K. and Adon, M. (2025) Relationship between Tropical Atlantic Marine Heatwaves and Rainfall in West Africa during the Monsoon Period. *Advances in Meteorology*, **2025**, Article ID: 7899901. https://doi.org/10.1155/adme/7899901

[8] Caniaux, G., Giordani, H., Redelsperger, J., Guichard, F., Key, E. and Wade, M. (2011) Coupling between the Atlantic Cold Tongue and the West African Monsoon in Boreal Spring and Summer. *Journal of Geophysical Research*, **116**, C04003. https://doi.org/10.1029/2010jc006570

[9] Zebiak, S.E. (1993) Air-Sea Interaction in the Equatorial Atlantic Region. *Journal of Climate*, **6**, 1567-1586. https://doi.org/10.1175/1520-0442(1993)006<1567:aiitea>2.0.co;2

[10] Keenlyside, N.S. and Latif, M. (2007) Understanding Equatorial Atlantic Interannual Variability. *Journal of Climate*, **20**, 131-142. https://doi.org/10.1175/jcli3992.1

[11] Philander, S.G.H. and Pacanowski, R.C. (1986) A Model of the Seasonal Cycle in the Tropical Atlantic Ocean. *Journal of Geophysical Research*: *Oceans*, **91**, 14192-14206. https://doi.org/10.1029/jc091ic12p14192

[12] Giordani, H. and Caniaux, G. (2014) Lagrangian Sources of Frontogenesis in the Equatorial Atlantic Front. *Climate Dynamics*, **43**, 3147-3162. https://doi.org/10.1007/s00382-014-2293-3

[13] Ruiz-Barradas, A., Carton, J.A. and Nigam, S. (2000) Structure of Interannual-to-Decadal Climate Variability in the Tropical Atlantic Sector. *Journal of Climate*, **13**, 3285-3297. https://doi.org/10.1175/1520-0442(2000)013<3285:soitdc>2.0.co;2

[14] Schouten, M.W., Matano, R.P. and Strub, T.P. (2005) A Description of the Seasonal Cycle of the Equatorial Atlantic from Altimeter Data. *Deep Sea Research Part I*: *Oceanographic Research Papers*, **52**, 477-493. https://doi.org/10.1016/j.dsr.2004.10.007

[15] Bourlès, B., Araujo, M., McPhaden, M.J., Brandt, P., Foltz, G.R., Lumpkin, R., *et al.* (2019) PIRATA: A Sustained Observing System for Tropical Atlantic Climate Research and Forecasting. *Earth and Space Science*, **6**, 577-616. https://doi.org/10.1029/2018ea000428

[16] Brandt, P., Alory, G., Awo, F.M., Dengler, M., Djakouré, S., Imbol Koungue, R.A., *et al.* (2023) Physical Processes and Biological Productivity in the Upwelling Regions of the Tropical Atlantic. *Ocean Science*, **19**, 581-601. https://doi.org/10.5194/os-19-581-2023

[17] Jouanno, J., Hernandez, O. and Sanchez-Gomez, E. (2017) Equatorial Atlantic Interannual Variability and Its Relation to Dynamic and Thermodynamic Processes. *Earth System Dynamics*, **8**, 1061-1069. https://doi.org/10.5194/esd-8-1061-2017

[18] Sultan, B. and Janicot, S. (2003) The West African Monsoon Dynamics. Part II: The "Preonset" and "Onset" of the Summer Monsoon. *Journal of Climate*, **16**, 3407-3427. https://doi.org/10.1175/1520-0442(2003)016<3407:twamdp>2.0.co;2

[19] Annamalai, H., Xie, S.P., McCreary, J.P. and Murtugudde, R. (2005) Impact of Indian Ocean Sea Surface Temperature on Developing El Niño. *Journal of Climate*, **18**, 302-319. https://doi.org/10.1175/jcli-3268.1

[20] Jouanno, J., Marin, F., du Penhoat, Y., Sheinbaum, J. and Molines, J. (2011) Seasonal Heat Balance in the Upper 100 M of the Equatorial Atlantic Ocean. *Journal of Geophysical Research*, **116**, C09003. https://doi.org/10.1029/2010jc006912

[21] Lübbecke, J.F., Rodríguez-Fonseca, B., Richter, I., Martín-Rey, M., Losada, T., Polo, I., *et al.* (2018) Equatorial Atlantic Variability—Modes, Mechanisms, and Global Teleconnections. *WIREs Climate Change*, **9**, e527. https://doi.org/10.1002/wcc.527

[22] Richter, I., Kido, S., Tozuka, T., Kosaka, Y., Tokinaga, H. and Chang, P. (2025) Revisiting the Inconsistent Influence of El Niño-Southern Oscillation on the Equatorial Atlantic. *Journal of Climate*, **38**, 481-496. https://doi.org/10.1175/jcli-d-24-0182.1

[23] Song, Q. and Aiki, H. (2023) Equatorial Wave Diagnosis for the Atlantic Niño in 2019 with an Ocean Reanalysis. *Ocean Science*, **19**, 1705-1717. https://doi.org/10.5194/os-19-1705-2023

[24] Drévillon, M., Lellouche, J.M., Régnier, C., Garric, G., Bricaud, C., Hernandez, O. and Bourdallé-Badie, R. (2022) Global Ocean Reanalysis Products GLOB-AL_REANALYSIS_PHY_001_030. EU Copernicus Marine Service. https://documentation.marine.copernicus.eu/QUID/CMEMS-GLO-QUID-001-030.pdf

[25] Petitgas, P., Doray, M., Huret, M., Massé, J. and Woillez, M. (2014) Modelling the Variability in Fish Spatial Distributions over Time with Empirical Orthogonal Functions: Anchovy in the Bay of Biscay. *ICES Journal of Marine Science*, **71**, 2379-2389. https://doi.org/10.1093/icesjms/fsu111

[26] Shields, C.A., DeSantis, D., Jonko, A., Lee, J., Caron, J.M., Phillips, A.S., *et al.* (2026) Challenges and Alternatives to Empirical Orthogonal Functions for Earth System Data. *Scientific Reports*, **16**, Article No. 18794. https://doi.org/10.1038/s41598-026-49505-z

[27] Knobler, S., Rilov, G., Garfinkel, C.I. and Liberzon, D. (2025) Climate Change Impacts in Eastern Mediterranean Sea: Trends and Extremes. *Water Waves*, **7**, 521-556. https://doi.org/10.1007/s42286-025-00118-5

[28] Garfinkel, C.I., Knobler, S., Liberzon, D. and Rilov, G. (2026) Precursors of Marine Heatwaves in the Eastern Mediterranean. *Geophysical Research Letters*, **53**, e2025GL120652. https://doi.org/10.1029/2025gl120652

[29] Amaya, D.J., Jacox, M.G., Alexander, M.A., Scott, J.D., Deser, C., Capotondi, A., *et al.* (2023) Bottom Marine Heatwaves along the Continental Shelves of North America. *Nature Communications*, **14**, Article No. 1038. https://doi.org/10.1038/s41467-023-36567-0

[30] Liess, S. and Bengtsson, L. (2004) The Intraseasonal Oscillation in ECHAM4 Part II: Sensitivity Studies. *Climate Dynamics*, **22**, 671-688. https://doi.org/10.1007/s00382-004-0407-z

[31] Holbrook, N.J., Scannell, H.A., Sen Gupta, A., Benthuysen, J.A., Feng, M., Oliver, E.C.J., *et al.* (2019) A Global Assessment of Marine Heatwaves and Their Drivers. *Nature Communications*, **10**, Article No. 2624. https://doi.org/10.1038/s41467-019-10206-z

[32] Mignot, J., Lazar, A. and Lacarra, M. (2012) On the Formation of Barrier Layers and Associated Vertical Temperature Inversions: A Focus on the Northwestern Tropical Atlantic. *Journal of Geophysical Research*: *Oceans*, **117**, C02010. https://doi.org/10.1029/2011jc007435